Supplementary Materials

Monolithically silicon photonic integrated transceiver for microwave and optical dual-band beamforming and free-space communications

Ruiqi Zheng[1,2], Jingxu Chen[1,2], Jinkun Hu[1,2], Haikun Huang[1,2], Junyi Zhang[1,2], Wufei Zhou[1,2], Sheng Dong[1,2], Xudong Wang[1,2], Xinhuan Feng[1,2], Jiejun Zhang[1,2*], Jianping Yao[1,3*]

1. International Cooperation Joint Laboratory for Optoelectronic Hybrid Integrated Circuits, Jinan University, Guangzhou, 511443, China,
2. College of Physics & Optoelectronic Engineering, Jinan University, Guangzhou 510632, China
3. Microwave Photonics Research Laboratory, School of Electrical Engineering and Computer Science, University of Ottawa, Ottawa, ON K1N 6N5, Canada
*Correspondence to: zhangjiejun@jnu.edu.cn, jpyao@uottawa.ca

Contents

S1. Fabrication Method

The silicon photonic chip was fabricated on a silicon-on-insulator (SOI) platform at the Advanced Micro Foundry (AMF). Key components including 14 grating couplers, 1×2 and 2×2 multimode interference (MMI) couplers, 36 thermo-optic phase shifters, 2 dual-parallel Mach-Zehnder modulators (DPMZM1 and DPMZM2) and 8 photodiodes (PDs) were designed using AMF's process design kit (PDK). The chip layout was designed using Luceda IPKISS photonic integrated circuit design software.

S2. Optical and Electrical Packaging

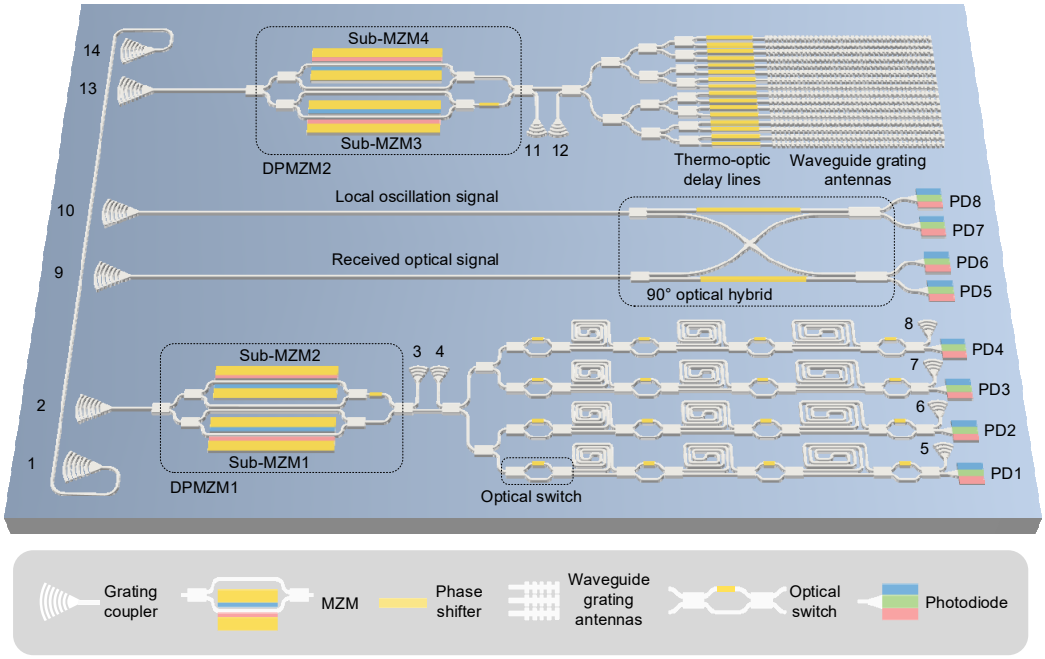

Figure S1. The schematic diagram of the transceiver incorporating a microwave TTD beamforming network, an OPA network and an optical coherent receiver for microwave and near-infrared dual-band free-space communication.

As shown in Fig. S1, the system employs 14 grating couplers for light coupling into or out of the chip (Ports 1 to 14). Port 1 and port 14, connected via a silicon waveguide, are used for measuring the coupling loss. Port 2 is used as the optical input port for the microwave true time delay (TTD) beamforming network. Port 3 is used as a test port for testing DPMZM1 (sub-MZM1 and sub-MZM2) within the microwave TTD beamforming network. Port 4 is used as an input port for calibrating the 4 optical switch delay lines (OSDLs), whereas ports 5~8 are used to perform delay lines calibration. Port 9 and port 10 are used as the input ports for the optical coherent receiver, receiving the communication optical signal and local oscillator (LO) signal, respectively. Port 13 is used as the optical input port for the optical phased array (OPA). Port 11 is used as a test port for testing DPMZM2 (MZM3 and MZM4) in the optical coherent transmitter. Port 12 is used as an input port for testing the OPA.

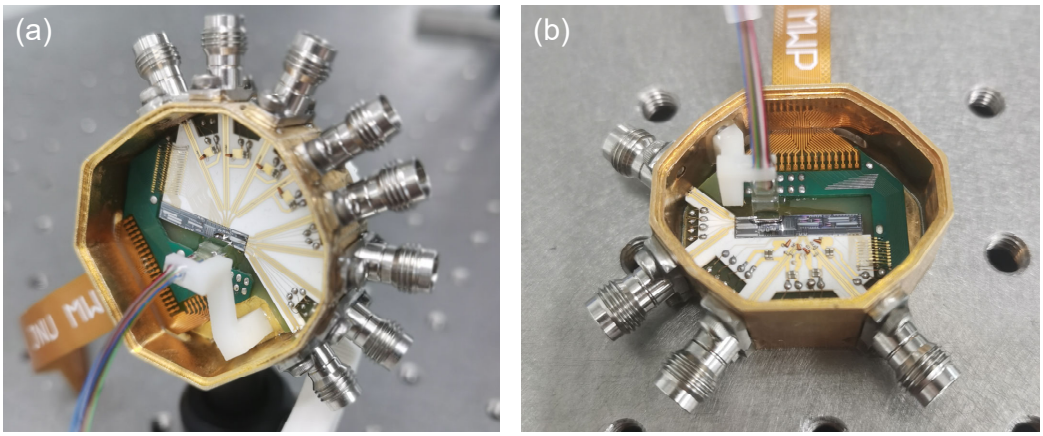

Figure S2. (a) Packaged dual-band transmitter including the microwave and optical beamforming networks. (b) Packaged coherent receiver.

The high-density integration of four modulators and eight PDs within the chip poses substantial challenges when consolidating the three subsystems within a single packaged module. This dense packaging leads to significant RF losses for both the modulators and the PDs, while also reducing their operational bandwidths. To ensure optimal performance of all on-chip components, we package the three subsystems into two separate modules, the transmitter module and the coherent receiver module. The transmitter module consists of the microwave TTD beamforming network and the OPA, as shown in Fig. S2(a). The receiver module has only the optical coherent receiver, as shown in Fig. S2(b). The optical packaging process primarily involves two key steps: 1) optimizing the alignment for high efficiency optical coupling and 2) UV-curing adhesive fixation. After packaging, we measure the coupling loss between port 1 and port 14, which are connected by a 2 mm waveguide. The total loss was 11 dB, indicating a coupling loss of approximately 5.5 dB per fiber-chip interface. Due to the high-density integration of multiple modulators and PDs on the chip, a high-dielectric-constant substrate is required to connect the RF electrodes on the chip to the external connectors while maintaining 50-Ω impedance matching. In the packaged modules, we employ alumina (Al_2O_3) as the substrate material, which offers a high dielectric constant ε_r of 9.9 and an ultra-low loss tangent $\tan\delta$ of 0.0001 for microwave signal transmission. The microstrip lines, fabricated using 2 μm gold traces, are optimized using HFSS simulations to ensure impedance matching and minimize signal reflection. To connect the RF electrodes to the microstrip lines, 25 μm diameter gold wire bonding is employed. Wire bonding is also used to connect the DC ports to the gold traces on the substrate. To reduce microwave losses at these interconnects, the chip and substrate are precisely aligned, and the RF electrodes on the chip are positioned in close proximity to the substrate, minimizing the wire bond lengths. A comparison of the magnitude responses of an on-chip MZM and PD before and after packaging is shown in Fig. S3(a) and S3(b), respectively. The degradation in the magnitude responses after packaging is primarily attributed to the wire bonding loss, the microstrip line loss, and the RF connector loss. The post-packaging 3-dB bandwidths are 16 GHz for the MZM and 17 GHz for the PD.

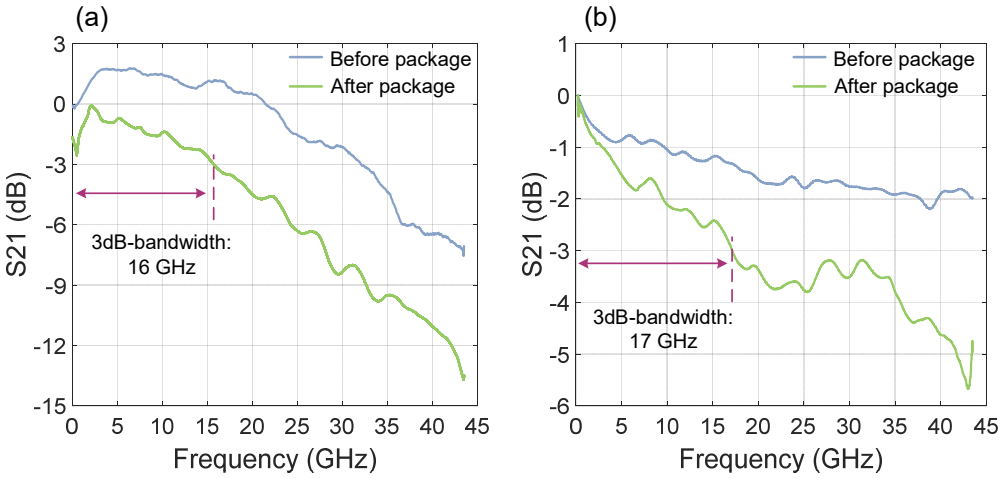

Figure S3. On-chip components characterization before and after packaging. (a) Measured magnitude response of an on-chip MZM. (b) Measured magnitude response of an on-chip PD. Blue curve: Pre-packaging measurement using RF probes. Green curve: Post-packaging measurement.

S3. Calibration of the Optical Switch Delay Lines

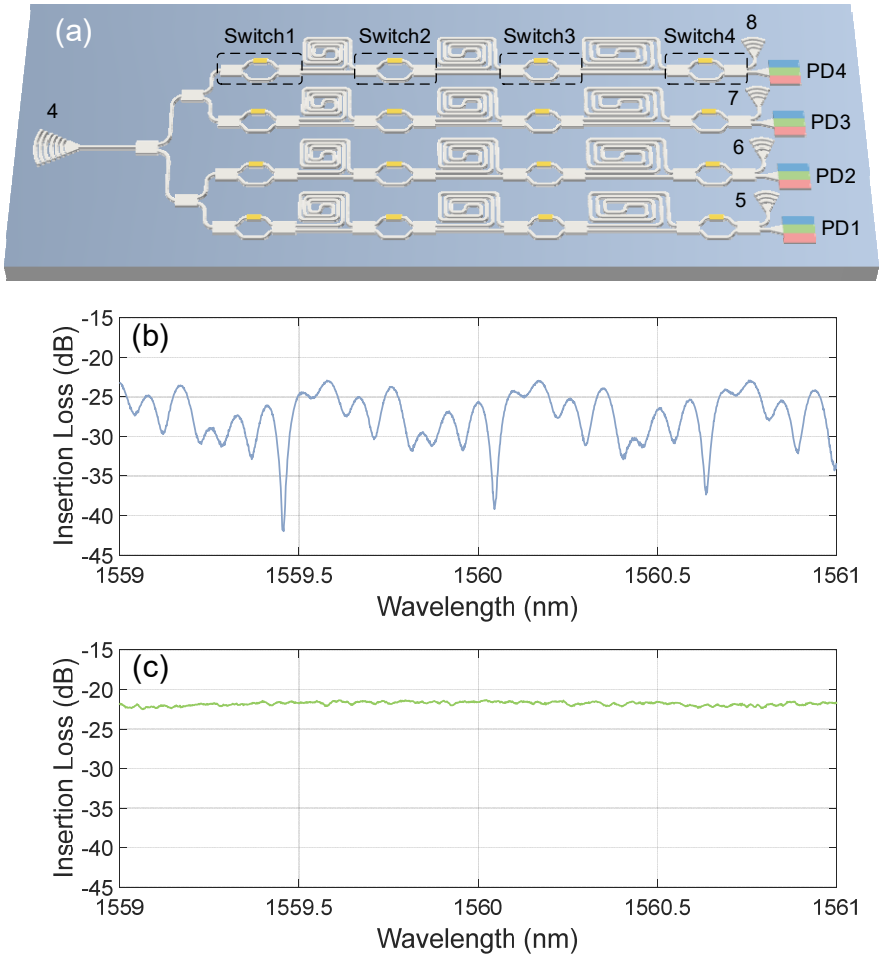

Figure S4. (a) The diagram of the microwave TTD beamforming network. (b) Optical spectral response measured before calibration. (c) Optical spectral response measured after calibration.

In the design of the microwave TTD beamforming network, all switches are in the cross states when no voltages are applied. However, due to fabrication errors, the switches are not exactly in the cross states. When measuring the spectral response of the upper OSDL between the output port (port 8) and the input port (port 4), as shown in Fig. S4(a), the spectral response has variations due to optical interferences, as shown in Fig. S4(b). A solution to eliminate the errors is to perform calibration. Following the calibration method proposed in [1], we tune the voltages applied to switches 1~4 to allow all switches to operate in the cross states, which In the design of the microwave TTD beamforming network, all switches are in the cross states when no voltages are applied. However, due to fabrication errors, the switches are not exactly in the cross states. When measuring the spectral response of the upper OSDL between the output port (port 8) and the input port (port 4), as shown in Fig. S4(a), the spectral response has variations due to optical interferences, as shown in Fig. S4(b). A solution to eliminate the errors is to perform calibration. Following the calibration method

proposed in [1], we tune the voltages applied to switches 1~4 to allow all switches to operate in the cross states, which results in a flat spectral response, as shown in Fig. S4(c).

The extinction ratios of the OSDLs in the microwave TTD beamforming network are also measured. To measure the extinction ratio of the upper OSDL, for example, all the switches in the OSDL are firstly calibrated to be in the bar state. The spectral response is shown as the solid black line in Fig. S5. Then, we change the state of one switch from bar state to cross state and measure the spectral response. For the four switches, four spectral responses are obtained, which are shown by the red, blue, green and pink lines in Fig. S5. As can be seen, the extinction ratio exceeds 20 dB over a 2 nm bandwidth.

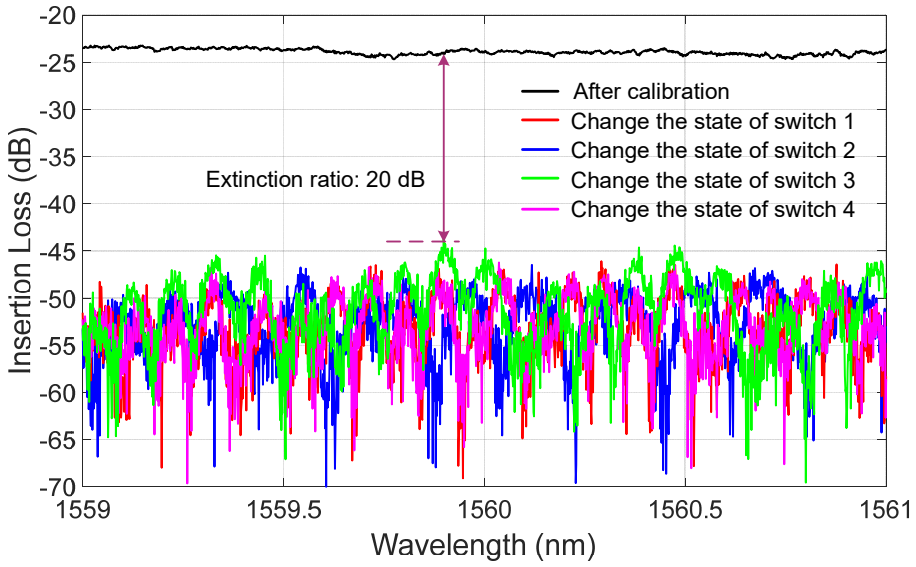

Figure S5. The extinction ratio measurements of the OSDL from part 4 to port 8.

S4. Delay Measurement of the Microwave True time delay Beamforming Network

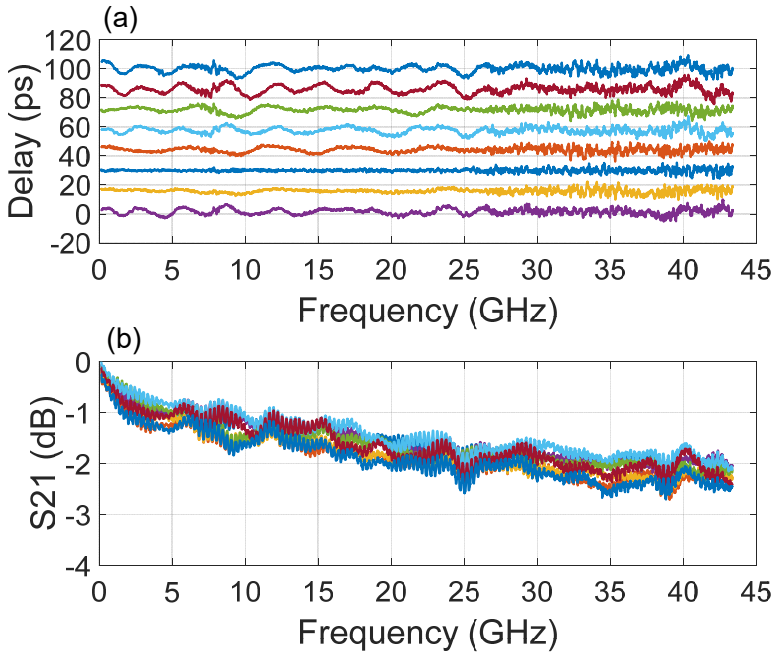

Figure S6. The measured (a) delay and (b) magnitude response of the OSDL.

To measure the time delays of the upper OSDL, an optical carrier modulated by a microwave signal is sent to the chip from port 4 via a grating coupler. The time delayed optical signal is applied to PD8. By changing the states of the optical switches, 8 different time delays are obtained. To maintain consistent optical input power to PD8 across these different time delays, the voltage applied to the fourth-stage optical switch is adjusted. This compensates for the insertion loss variation caused by the different waveguide lengths associated with each specific time delay. Figure S6(a) shows the measured time delays. As can be seen, the delay lines can provide 8 tunable time delays from 0–98 ps with a tuning step of 14 ps over a wide frequency range from 10 MHz to 43.5 GHz. The magnitude responses of the delay lines for different time delays are also measured, as shown in Fig. S6(b). The difference between the magnitude responses is below 1 dB.

S5. The Calibration of the Optical Phased Array

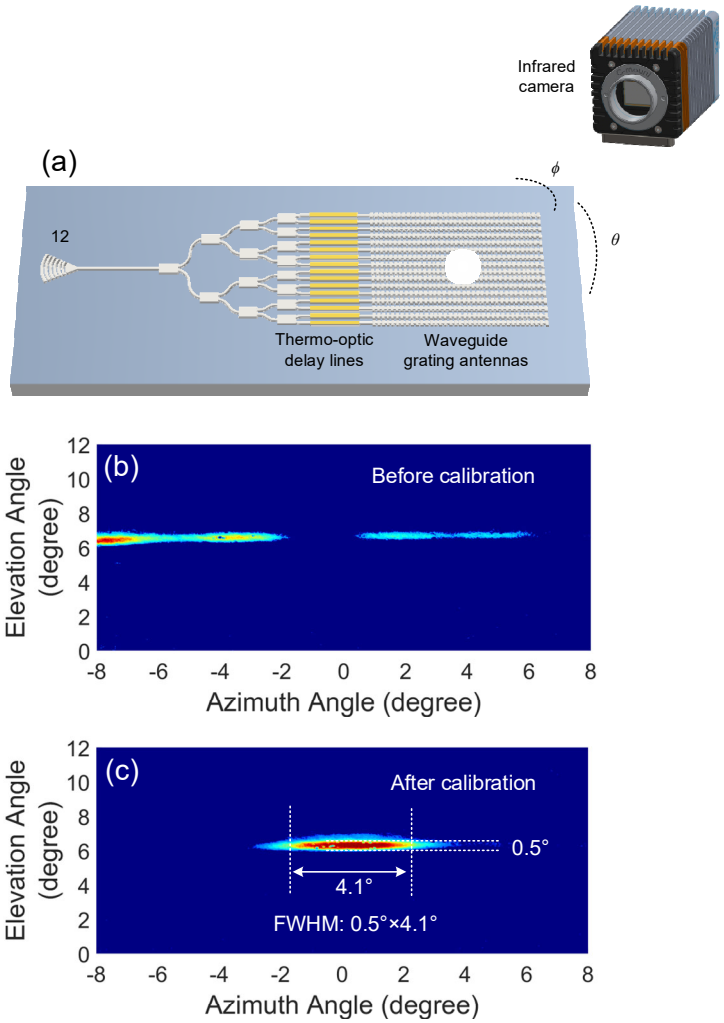

Figure S7. (a) The diagram of the OPA. (b) Optical spot measured before calibration. (c) Optical spot measured after calibration.

In the OPA system, fabrication-induced variations introduce initial delay mismatches among the sixteen waveguide delay lines, preventing the formation of a well-focused laser beam due to unmet phase-matching conditions. Therefore, calibration is needed. During the calibration, a continuous-wave (CW) light is coupled into the chip from port 12 via a grating coupler. The voltages applied to the sixteen thermo-optic delay lines are adjusted to minimize the initial delay difference, while an infrared (IR) camera is used to monitor the intensity profile of the beam in real time, as shown in Fig. S7(a). The calibration is deemed complete when the beam reaches maximum energy concentration. As seen in Fig. S7(b), without calibration, the beam energy is dispersed into multiple spots, indicating significant energy divergence. After calibration, as shown in Fig. S7(c), the energy converges into a spot with a full-width at half-maximum (FWHM) of 0.5° × 4.1°. By increasing the number of delay lines, the FWHM of the optical beam could be further reduced [2].

S6. Characterization of the Optical Coherent Transmitter and Receiver

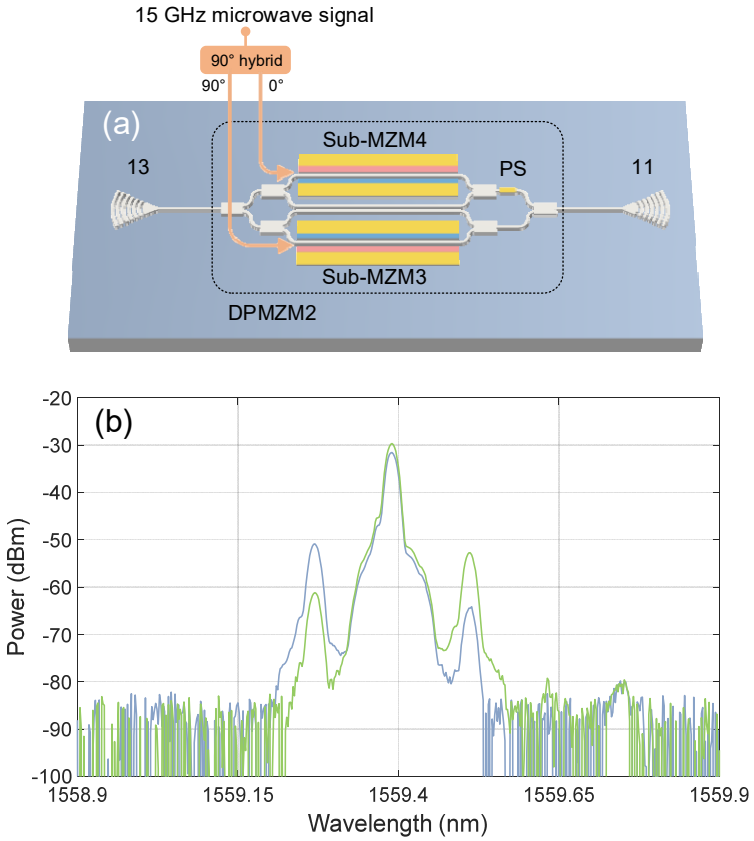

Figure S8. (a) The diagram of DPMZM2. (b) The measured optical spectra of the single sideband with carrier (C+SSB) modulation at port 11.

The optical coherent transmitter employs a dual-parallel Mach-Zehnder modulator (DPMZM2), comprising two sub-Mach-Zehnder modulators (sub-MZM3 and sub-MZM4) and a thermal phase shifter (PS), as shown in Fig. S8(a). To verify the operation of the DPMZM2, a CW light is coupled into the chip from port 13 via a grating coupler. A 15 GHz microwave signal generated by an external microwave source is input to a 90° hybrid coupler, producing two microwave signals with a 90° phase difference. These two microwave signals are applied to sub-MZM3 and sub-MZM4 respectively. The voltage applied to the PS is adjusted to introduce a $\pi/2$ phase difference between upper and lower branch of DPMZM2 to realize single sideband with carrier (C+SSB) modulation. The optical spectra are measured at port 11, and are shown in Fig. S8(b). The blue line and the green line show the optical spectra of C+SSB modulation when a $\pi/2$ phase difference and a $-\pi/2$ phase difference are introduced, respectively. The results shown in Fig. S8(b) demonstrate that DPMZM2 can work properly.

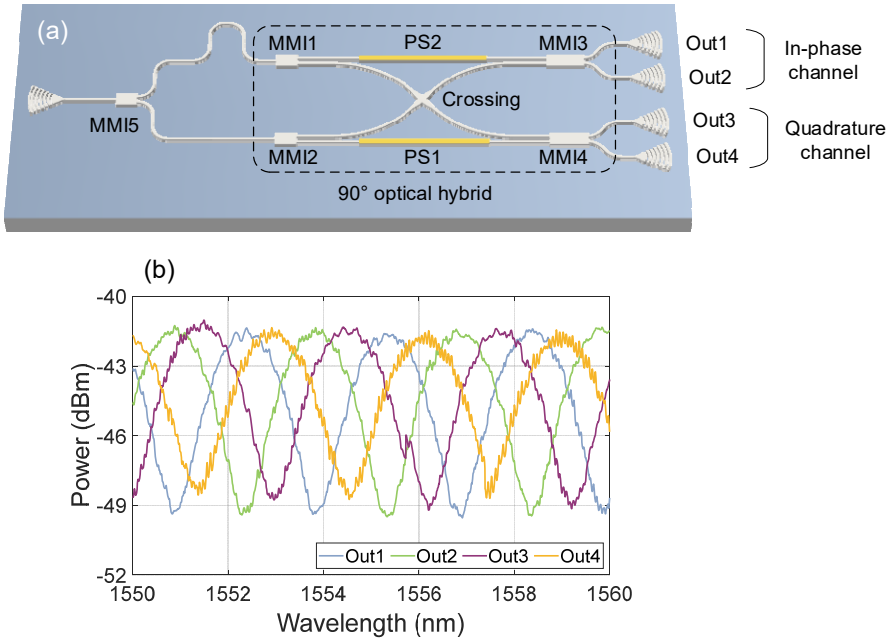

Figure S9. (a) The schematic diagram of a test 90° optical hybrid. (b) The measured spectral responses at the four output ports of the 90° optical hybrid.

The optical coherent receiver consists of two key components: a 90° optical hybrid and two balanced photodetectors (BPDs). To test the 90° optical hybrid, a separate 90° optical hybrid is designed, as shown Fig. in S9(a). The 90° optical hybrid is implemented using two 1×2 multimode interferometers (MMI1 and MMI2), two 2×2 MMIs (MMI3 and MMI4), a waveguide crossing and two thermal phase shifters (PS1 and PS2), while the BPDs are implemented using two discrete PDs with external circuit designed to subtract the output signals from the two PDs. To characterize the performance of the 90° optical hybrid, a broadband optical signal generated by an optical vector analyzer (OVA) is coupled into the chip via a grating coupler. This signal is split into two equal parts via a 3-dB optical coupler (MMI5) and fed into the hybrid, as shown in Fig. S9(a), with a controlled optical path delay difference between the two paths. Figure S9(b) presents the measured optical spectra at the four output ports of the hybrid, exhibiting sinusoidal interference patterns due to the phase difference induced by the delay. By tuning the two PSs within the hybrid, we enforce the required quadrature phase relationship between the outputs. The results clearly demonstrate the orthogonality between the in-phase (Out1 & Out2) and quadrature (Out3 & Out4) paths and also demonstrate a π-phase shift within the in-phase pair (Out1 vs. Out2) and the quadrature pair (Out3 vs. Out4). These measurements confirm the proper operation of the 90° optical hybrid, validating its capability for coherent detection.

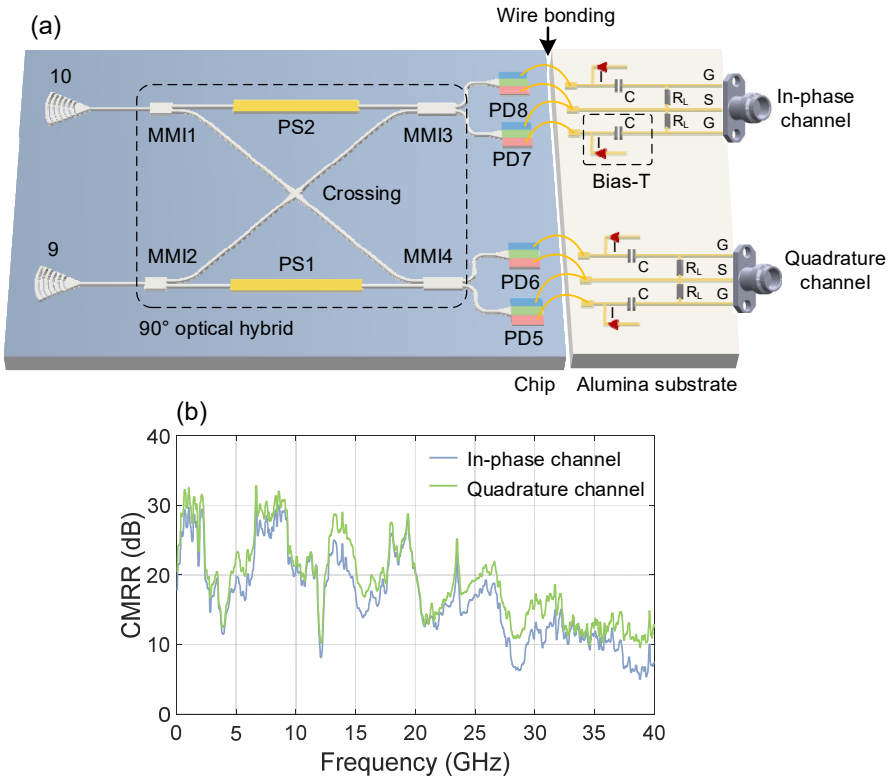

Figure S10. (a) The schematic diagram of the optical coherent receiver. (b) the measured common-mode rejection ratio (CMRR). I: inductance, C: capacitance, R_L: load resistance, G: ground, S: signal.

In the packaged modules, the BPDs are implemented on the chip and the outputs are connected to the microstrip lines on an external alumina substrate as shown in Fig. S10(a), which is designed according to [3]. To verify the functionality of these two BPDs, an optical carrier modulated with a microwave signal is coupled into the chip through port 10. After passing through the 90° optical hybrid, the optical signal is split into four parts and applied to PD5, PD6, PD7, and PD8. The signal of the in-phase channel is obtained by subtracting the signals from PD5 and PD6 using a circuit on the alumina substrate. Similarly, the signal of the quadrature channel is obtained by subtracting the signals from PD7 and PD8 using a circuit on the alumina substrate. The measured common-mode rejection ratio (CMRR) of the in-phase channel and quadrature channel are shown by the blue curve and green curve in Fig. S10(b), respectively. The CMRR exhibits significant degradation around 4 GHz and 12 GHz, which could be attributed to impedance mismatch in the external circuitry. Excluding the dip at 12 GHz, the bandwidth with CMRR >10 dB reaches 27.5 GHz. The experimental results shown in Fig. S10(b) demonstrate that these two BPDs can work properly.

References

[1] S. Shi *et al.*, "Non-invasive delay state calibration of silicon optical switching delay line," *J. Lightwave Technol.,* vol. 40, pp. 1-10, 10/01 2022.

[2] C. Poulton *et al.*, "Large-scale silicon nitride nanophotonic phased arrays at infrared and visible wavelengths," *Opt. Lett.,* vol. 42, pp. 21-24, 12/20 2016.

[3] H.-G. Bach, "Ultra-broadband photodiodes and balanced detectors towards 100 Gbit/s and beyond," *Proc. SPIE Int. Soc. Opt. Eng.,* vol. 6014, 10/01 2005.